Opto-Electronic Advances

CN 51-1781/TN ISSN 2096-4579 (Print) ISSN 2097-3993 (Online)

Racemic dielectric metasurfaces for arbitrary terahertz polarization rotation and wavefront manipulation

Jie Li, Xueguang Lu, Hui Li, Chunyu Song, Qi Tan, Yu He, Jingyu Liu, Li Luo, Tingting Tang, Tingting Liu, Hang Xu, Shuyuan Xiao, Wanxia Huang, Yun Shen, Yan Zhang, Yating Zhang and Jianquan Yao

Citation: Li J, Lu XG, Li H, et al. Racemic dielectric metasurfaces for arbitrary terahertz polarization rotation and wavefront manipulation. *Opto-Electron Adv* **7**, 240075(2024).

https://doi.org/10.29026/oea.2024.240075

Received: 2 April 2024; Accepted: 1 July 2024; Published online: 28 August 2024

Opto-Electronic Advances

Article

October 2024, Vol. 7, No. 10

DOI: 10.29026/oea.2024.240075

Racemic dielectric metasurfaces for arbitrary terahertz polarization rotation and wavefront manipulation

Jie Li[1,2], Xueguang Lu[3], Hui Li[2], Chunyu Song[2], Qi Tan[2], Yu He[1], Jingyu Liu[6], Li Luo[1], Tingting Tang[1], Tingting Liu[4], Hang Xu[2]*, Shuyuan Xiao[4]*, Wanxia Huang[3]*, Yun Shen[5]*, Yan Zhang[6], Yating Zhang[2] and Jianquan Yao[2]*

Dielectric chiral metasurface is a new type of planar and efficient chiral optical device that shows strong circular dichroism or optical activity, which has important application potential in optical sensing and display. However, the two types of chiral optical responses in conventional chiral metasurfaces are often interdependent, as their modulation of the amplitudes and phases of orthogonal circularly polarized components is correlated, which limits the further progress of chiral meta-devices. Here we propose a new scheme for independently designing the circular dichroism and optical activity of chiral metasurfaces to further control the polarization and wavefront of transmitted waves. Inspired by mixtures of chiral molecular isomers, we use the dielectric isomer resonators to form “super-units” instead of single meta-atoms for chiral responses in terahertz band, which is called racemic metasurface. By introducing two levels of Pancharatnam-Berry phases between meta-atoms and “super-units”, the polarization rotation angle and wavefront of the beam can be designed without the far-field circular dichroism. We demonstrate the strong control ability on terahertz waves of this scheme through simulation and experiments. In addition, this new type of device with near-field chirality but no far-field circular dichroism may also have important value in optical sensing and other technologies.

Keywords: racemic; dielectric metasurfaces; terahertz waves; chirality

Li J, Lu XG, Li H et al. Racemic dielectric metasurfaces for arbitrary terahertz polarization rotation and wavefront manipulation. *Opto-Electron Adv* **7**, 240075 (2024).

Introduction

The arbitrary control of light waves or photons is a core topic for modern optics and photonics, and it is also the foundation of optical devices and systems[1]. In recent decades, the rapid development of ultrafast laser, quantum optics, Fourier optics and other fields has promoted

[1]College of Optoelectronic Engineering, Chengdu University of Information Technology, Chengdu 610225, China; [2]School of Precision Instruments and Opto-Electronics Engineering, Tianjin University, Tianjin 300072, China; [3]College of Materials Science and Engineering, Sichuan University, Chengdu 610065, China; [4]School of Information Engineering, Nanchang University, Nanchang 330031, China; [5]Department of Physics, School of Physics and Materials Science, Nanchang University, Nanchang 330031, China; [6]Key Laboratory of Terahertz Optoelectronics, Ministry of Education, Department of Physics, Capital Normal University, Beijing 100048, China.

*Correspondence: H Xu, E-mail: xh_931119@tju.edu.cn; SY Xiao, E-mail: syxiao@ncu.edu.cn; WX Huang, E-mail: huangwanxia@scu.edu.cn; Y Shen, E-mail: shenyun@ncu.edu.cn; JQ Yao, E-mail: jqyao@tju.edu.cn

Received: 2 April 2024; Accepted: 1 July 2024; Published online: 28 August 2024

the new applications of laser and terahertz wave such as communication, imaging, and advanced manufacturing[2]. However, with the growing demand for diversified and intelligent optical systems, the number and complexity of optical devices are increasing, posing higher requirements for their integration level and optical field control dimension. Traditional optical devices such as lenses, wave plates and polarizers are bulky and highly dependent on the characteristics of their constituent materials. It is difficult for a single device to achieve multi-dimensional manipulation of light, and many optical components require precise processing or human experiences. In the past decade, nanophotonics and metasurfaces have provided an important alternative solution for this problem[3–5]. The planar and ultra-thin structures of optical metasurfaces are conducive to the efficient integration of multiple devices, and their preparation methods are in line with the progress of modern micro/nano processing technology[6,7]. More importantly, dual- or even multi-parameters control of light such as amplitude, phase, polarization and wavefront can be achieved via a single meta-device[8–10]. It provides important ways for emerging fields such as manipulation of photon state[11,12], light control in momentum space[13,14], and micro-nano laser sources[15,16].

Chiral nanophotonics is an important part of the micro-nano optics, and its achievements have covered light sources[17,18], optical devices and photodetectors[19–22]. The chiral optical responses in metasurfaces include optical activity (OA) and circular dichroism (CD), which are obtained through intrinsic or extrinsic chirality[23,24]. Electromagnetic resonances can be selectively excited by circularly polarized light in chiral meta-atoms to generate optical chirality much greater than free space wave at the micro-nano scale, which have been applied in biochemical sensing[25], circularly polarized light detection[26], optical display[27], and other scenarios[28]. Combined with Pancharatnam-Berry (P-B) phase, its polarization sensitive far-field control capability can be used for multi-channel holography, full space beam focusing and dynamic polarization modulation[29–33]. The optical activity and circular dichroism of intrinsic chiral meta-atoms can be considered as originating from differences in real and imaginary parts of their equivalent refractive indices (caused by electromagnetic mode in subwavelength scale) for left and right circularly polarized (LCP and RCP) waves, resulting in differences in their phase and amplitude[34]. For a single chiral meta-atom, achieving controllable OA without CD in far-field region by adjusting structural parameters is difficult, as the rotation of polarization angle are often accompanied by changes in the amplitude of the orthogonal circularly polarized components, i.e. changes in ellipticity[35]. How to obtain arbitrary polarization rotation without CD using chiral metasurfaces while designing other optical parameters simultaneously is still an attractive topic. Specifically, chiral metasurfaces in terahertz band can achieve novel applications such as dynamic polarization manipulation and biochemical sensing[36–44].

In this paper, we propose a new method for arbitrary polarization rotation and wavefront manipulation based on racemic dielectric metasurfaces, inspired by the mixture of chiral molecular isomers. Without loss of generality, we demonstrate an example of all-silicon meta-device in the terahertz band. By combining a pair of isomers with mirror patterns to form a "super-unit" instead of a single chiral meta-atom, arbitrary polarization rotation angles are obtained while maintaining almost constant ellipticity. At the same time, relative phase shift is introduced between the "super-units" based on P-B phase, and the wavefront of the transmitted wave is also can be designed. In addition, the racemic dielectric metasurfaces can still be excited for enhanced chiral near-field, but it does not show circular dichroism in the far-field region. We do not choose metal meta-atoms here, mainly considering that dielectric metasurfaces can provide high transmission efficiency while stimulating strong chiral responses, and are more conducive to the independent existence of chiral near-field near the two isomers. This novel characteristic may not only plays an important role for light field manipulation, but also has the potential to be applied in the sensing of chiral biochemical substances.

Results and discussion

The new scheme for polarization and wavefront manipulation based on racemic dielectric metasurface is shown in Fig. 1. Here, meta-devices in the terahertz band are used as demonstration examples, and we can design the transmitted wave for a specific wavefront (such as beam deflection, focusing and vortex generation) with arbitrary polarization rotation angle. A basic unit of a racemic metasurface consists of a pair of S-shaped chiral isomers, totaling four chiral meta-atoms as a “super-unit”. The metasurface is an all-silicon device, with both the substrate and upper structure composed of high

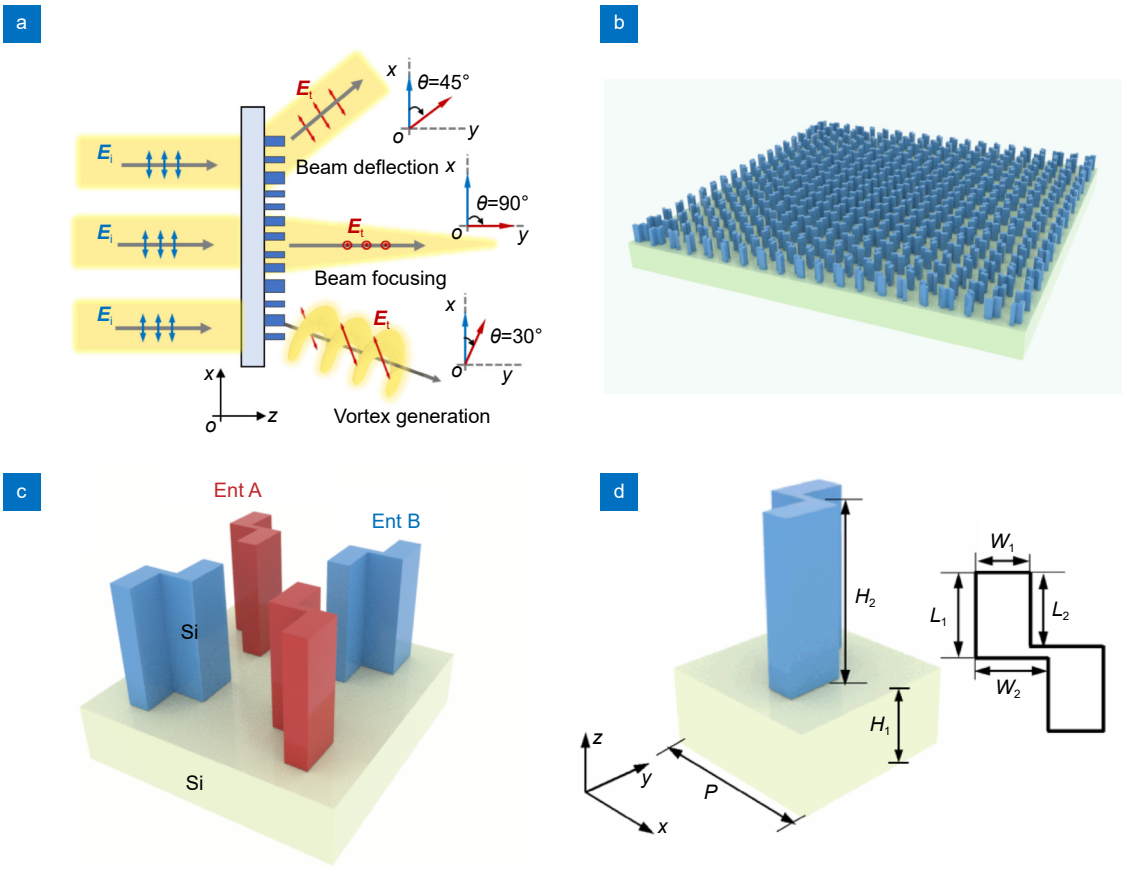

Fig. 1 | (**a**) Arbitrary polarization rotation and wavefront control capability of the device, such as beam deflection, focusing and vortex generation with different polarization rotation angles. (**b**) The array structure of a meta-device consisting of "super-units", where the chiral meta-atoms are rotated with different angles. (**c**) The composition of a "super-unit", where the red and blue parts respectively represent two different chiral meta-atoms (enantiomer A and enantiomer B, Ent A and Ent B). (**d**) The geometric parameters of the chiral meta-atoms, which are applicable to both Ent A and Ent B.

resistance silicon (ρ>20000 Ω). The geometrical parameters are shown in the figure, with substrate thickness H_1=300 μm, resonance unit height H_2=200 μm, period P=216 μm, and other in-plane dimensions L_1=72 μm, L_2=60 μm, W_1=36 μm, W_2=56 μm. All the samples we will demonstrate in the subsequent sections are composed of 30×30 "super-units" or 60×60 chiral meta-atoms.

The prerequisite for above functions is to obtain sufficient transmission circular dichroism (TCD) in chiral meta-atoms. By simulating and optimizing the S-shaped structure, we have found the size values listed earlier. We calculated four transmission coefficients using commercial software, as shown in Fig. 2(a) and 2(b), where the illustrations represent the corresponding unit shapes. The transmitted and incident terahertz waves can be correlated by the Jones matrix of meta-atoms[45]:

$$\begin{pmatrix} E_{\rm t}^x \\ E_{\rm t}^y \end{pmatrix} = \begin{pmatrix} t_{xx} & t_{xy} \\ t_{yx} & t_{yy} \end{pmatrix} \begin{pmatrix} E_{\rm i}^x \\ E_{\rm i}^y \end{pmatrix} = \boldsymbol{T} \begin{pmatrix} E_{\rm i}^x \\ E_{\rm i}^y \end{pmatrix}, \quad (1)$$

where $E_{i,j}^{x,y}$ are different incident and transmitted polarized electric fields, $t_{i,j(i,j=x,y)}$ are transmission coefficients in linear polarization basis. Based on the simulation results of transmission matrix $\boldsymbol{T}$, we calculate the transmission matrix for circularly polarized waves

$$\begin{pmatrix} t_{\rm RR} & t_{\rm RL} \\ t_{\rm LR} & t_{\rm LL} \end{pmatrix} = \frac{1}{2} \begin{pmatrix} t_{xx}+t_{yy}+{\rm i}(t_{xy}-t_{yx}) & t_{xx}-t_{yy}-{\rm i}(t_{xy}+t_{yx}) \\ t_{xx}-t_{yy}+{\rm i}(t_{xy}+t_{yx}) & t_{xx}+t_{yy}-{\rm i}(t_{xy}-t_{yx}) \end{pmatrix}, \quad (2)$$

where $t_{i,j(i,j=\rm R,L)}$ are transmission coefficients in circular polarization basis. The red unit shows strong TCD at the frequency of 1 THz, and the $t_{\rm RL}$ component in its transmission coefficients has the maximum value while the other quantities are very small. The situation for a blue unit is exactly opposite, with its $t_{\rm LR}$ component showing the maximum value. In addition, we also need the selected structure to be used for standard chiral geometric

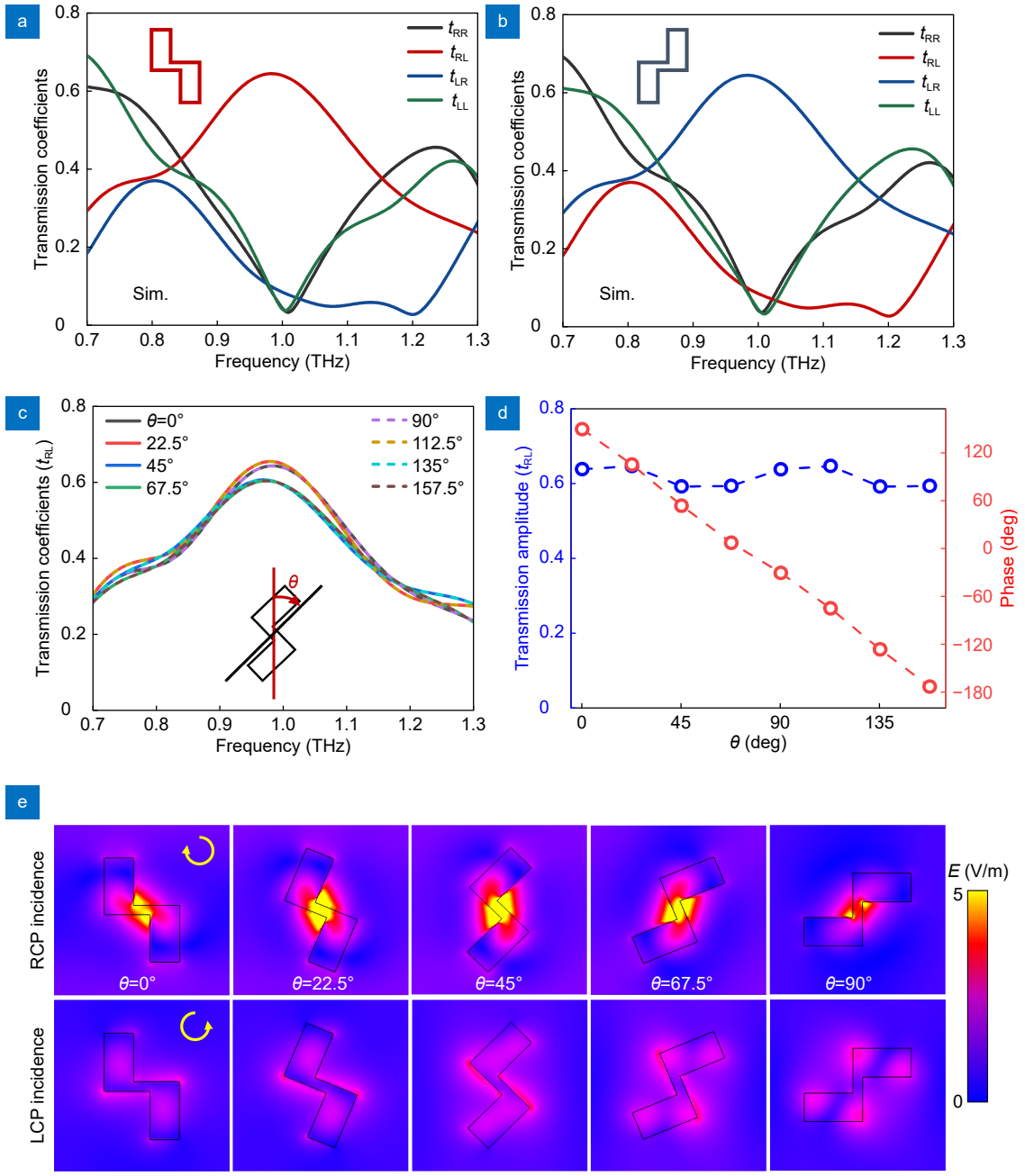

Fig. 2 | (**a**, **b**) Circularly polarized transmission coefficients of the chiral enantiomers. (**c**) The transmission component t_{RL} of the meta-atoms with different rotation angles. (**d**) The transmission amplitude and phase of chiral meta-atoms with different rotation angles at the operating frequency of 1 THz. (**e**) The localized electric field excited by LCP and RCP waves of meta-atoms with different rotation angles.

phase, as not all chiral meta-atoms can obtain P-B phase through rotation[29–33]. Figure 2(c) shows the transmission amplitude (t_{RL} component) and rotation angle of the aforementioned red unit after in-plane rotation around its geometric center. The step size of the rotation angle θ is 22.5 degrees. Obviously, these curves only show slight fluctuations and remained above 0.6 at the peak of the curve. More intuitively, we extracted the transmission amplitude and phase at different rotation angles at a frequency of 1 THz and displayed them in Fig. 2(d). It can be observed that the phase change satisfies good linearity, and we have obtained the standard chiral geometric phase. On the other hand, the spin selective transmission is mainly due to the high-order electric multipole excited by specific circularly polarized terahertz waves in chiral meta-atoms, which exhibit significant backward scattering. To prove this, we present the electric field distribution of the "red" meta-atoms under LCP and RCP

waves excitations in Fig. 2(e), where there is a significant electric field enhancement when RCP waves are incident, while LCP waves are almost unable to excite localized strong electric fields. More importantly, this selective enhancement can be almost maintained when the meta-atoms undergo in-plane rotation, which is also the direct reason for the appearance of chiral geometric phases.

We prepared the metasurface samples mentioned in Fig. 2(a) and 2(b) using standard UV lithography and ICP (Inductively Coupled Plasma) etching techniques. The samples with a same size of 1.4 cm × 1.4 cm are composed of meta-atoms without rotation (θ=0°). Scanning electron microscope (SEM) images of the structure (red unit) are presented in Fig. 3(a), and several photos from different perspectives and magnifications demonstrate the standardization of our sample preparation. We use a home-built polarization resolved terahertz time-domain spectroscopy (PTDS) system to measure the chiral transmission spectra of the samples, which contains four metal wire grid polarizers based on the standard TDS system. As shown in Fig. 3(b), by rotating polarizers P_2 and P_3 to 45° and −45° as new reference frames, four linearly polarized transmission coefficients are measured and then the circularly polarized transmission matrix are calculated according to Eq. (2). In the optical path, P_1 and P_4 are used to improving the polarization purity and enhancing measurement accuracy, where P_2 and P_3 are used for polarization projection. More detailed operating methods and theoretical basis can be seen in the Supplementary information Section 2. Figure 3(c) and 3(d) show the final experimental results, with the sample structures shown in red and blue patterns, respectively. The four circularly polarized transmission coefficients are in good agreement with the simulation results in Fig. 2, and there is a slight shift in the peak frequency, which may be a deviation generated during the sample etching process.

Then we will demonstrate the function of "super-units". Based on the transmission coefficients in Fig. 2(a) and 2(b), we calculated the transmission circular dichroism T_{CD} of the two mirror units using the following equation:

$$T_{CD} = |t_{RL}|^2 + |t_{LL}|^2 - |t_{LR}|^2 - |t_{RR}|^2 . \quad (3)$$

It can be seen in Fig. 4(a) and 4(b) that the peak value of enantiomer A in the curve is positive, with a maximum value close to 0.4. On the contrary, the peak value of enantiomer B is around −0.4. This already means high chirality efficiency, after all, terahertz waves show significant reflection losses at the air-silicon interface. It is

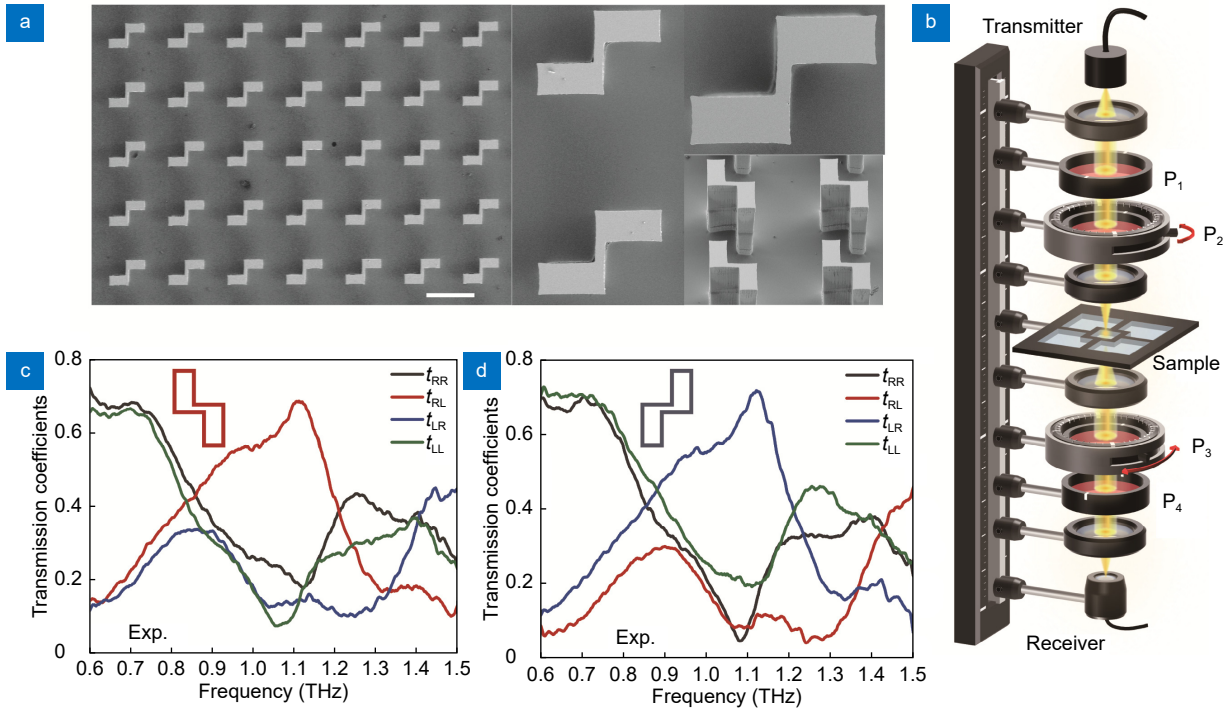

Fig. 3 | (**a**) Scanning electron microscopy (SEM) images of the chiral metasurface sample, the scale bar is 200 μm. (**b**) Schematic diagram of the polarization resolved terahertz time-domain spectroscopy system. (**c**, **d**) Measured results of the circularly polarized transmission spectra for two chiral metasurfaces.

interesting that when we combine the two enantiomers, the new "super-unit" in Fig. 4(c) becomes a racemic structure without circular dichroism because it has a mirror symmetry axis. Meanwhile, we present the near-field excitation of the three units mentioned above at 1 THz in Fig. 4(d–f). Compared with a single chiral meta-atom, the chiral near-field excited in hybrid structures has slightly weakened, but still maintains significant spin selectivity, providing assurance for the manipulation of transmitted waves.

In fact, enantiomers A and B serve as circular polarizers in the hybrid structure. When we introduce geometric phase by rotating the meta-atom, the transmitted orthogonal circularly polarized components combine to form a controllable rotated linearly polarized wave, which means the symmetry of the racemic structure has been disrupted. This can be analyzed from the classical polarization theory. Assuming that the transmitted components of two chiral isomers are RCP and LCP waves, with an initial phase of 0 and a rotation angle of red meta-atoms β. The two orthogonal components can be written by a Jones matrix as[46]:

$$\boldsymbol{E}_{\mathrm{L}}=\frac{1}{2}\begin{bmatrix}1\\ \mathrm{i}\end{bmatrix}\exp(\mathrm{i}\varphi_{\mathrm{L}}),\boldsymbol{E}_{\mathrm{R}}=\frac{1}{2}\begin{bmatrix}1\\ \mathrm{i}\end{bmatrix}\exp[\mathrm{i}(\varphi_{\mathrm{R}}+2\beta)]\ , \tag{4}$$

where φ_{R} and φ_{L} are phase shifts of circularly polarized components caused by the metasurface. The Jones vector of the terahertz wave synthesized after passing through a metasurface can be written as

$$\begin{aligned}\boldsymbol{E}=&\frac{1}{2}\begin{bmatrix}1\\ \mathrm{i}\end{bmatrix}\exp(\mathrm{i}\varphi_{\mathrm{L}})+\frac{1}{2}\begin{bmatrix}1\\ -\mathrm{i}\end{bmatrix}\exp[\mathrm{i}(\varphi_{\mathrm{R}}+2\beta)]\\ =&\frac{1}{2}\exp\left[\frac{\mathrm{i}}{2}(\varphi_{\mathrm{L}}+\varphi_{\mathrm{R}}+2\beta)\right]\\ &\cdot\left\{\begin{bmatrix}1\\ -\mathrm{i}\end{bmatrix}\exp(\mathrm{i}\beta)+\begin{bmatrix}1\\ \mathrm{i}\end{bmatrix}\exp(-\mathrm{i}\beta)\right\}.\end{aligned} \tag{5}$$

Make $\psi=(\varphi_{\mathrm{L}}+\varphi_{\mathrm{R}}+2\beta)/2$, and

$$\begin{aligned}\boldsymbol{E}=&\exp[\mathrm{i}\psi]\begin{bmatrix}\frac{1}{2}[\exp(\mathrm{i}\beta)+\exp(-\mathrm{i}\beta)]\\ \frac{1}{2}[\exp(\mathrm{i}\beta)-\exp(-\mathrm{i}\beta)]\end{bmatrix}\\ =&\exp[\mathrm{i}\psi]\begin{bmatrix}\cos\beta\\ \sin\beta\end{bmatrix}.\end{aligned} \tag{6}$$

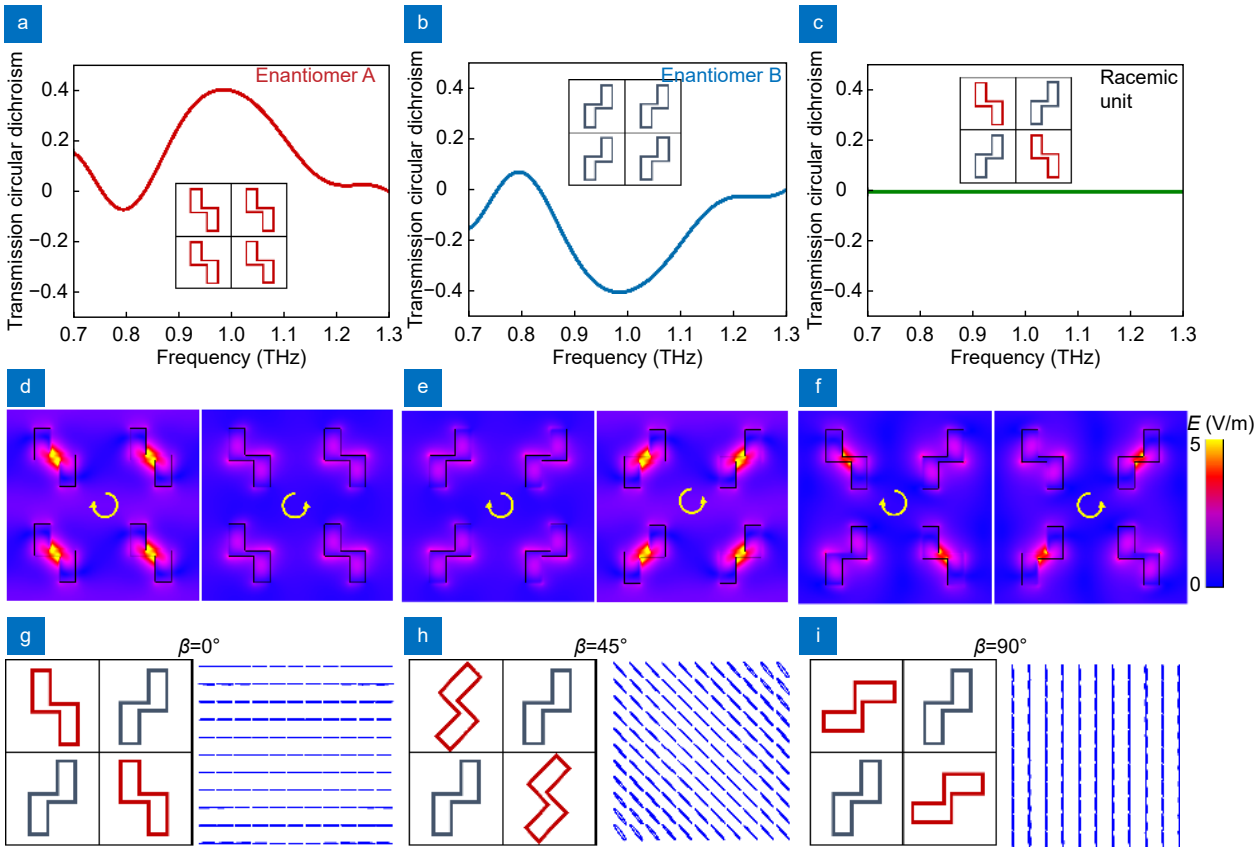

Fig. 4 | (**a–c**) Simulation results of the transmission circular dichroism for three types of super-units. (**d–f**) Local electric field excited by circularly polarized waves at 1 THz for three types of super-units. (**g–i**) Super-units with different rotation angles and the simulation results of their optical rotation function (β= 0°, 45°, and 90°).

Obviously, the rotation angle of the synthesized linearly polarized wave is equal to the in-plane rotation angle of the chiral unit, which provides a very convenient method for polarization manipulation. Of course, the rotation angle of unit here is a relative value, and different absolute angles can be used to design the transmitted wavefront. We have shown three examples in Fig. 4(g–i), assuming that the rotation angle of the red unit is β. The incident wave in the simulation is horizontally polarized (along the x-axis). The figure provides unit diagrams for each scenario and the polarization state of the transmitted wave, when β=0°, the polarization state of the transmitted wave is consistent with that of the incident wave. When β=45° or β=90°, the polarization state of the transmitted wave rotates by a corresponding angle.

Based on the above results, we can now achieve the final functionality of the meta-device. Firstly, we simulate the polarization rotation performance of a "super-unit" with a relative rotation angle of 90 degrees, as shown in Fig. 5(a). The incident x-polarized terahertz wave is efficiently converted into y-polarized at near f=1 THz. Based on the structure shown in Fig. 5(a), we assume that the angles at which the red and blue chiral meta-atoms rotate clockwise and counterclockwise, respectively, are β_1, then the relative phase shift obtained by the super-unit is φ=2β_1. We refer to the relative phase between super-units as the second-order Pancharatnam-Berry phase to distinguish the phase shift between the red and blue units mentioned earlier (first-order Pancharatnam-Berry phase). Figure 5(b) shows several different scenarios. Without loss of generality, we take focusing beams as an example to demonstrate the functions of our metasurface. Figure 5(c) shows the phase profile required for focusing, calculated by the following equation:

$$\varphi(x,y) = -\frac{2\pi}{\lambda}\left(\sqrt{x^2+y^2+f^2}-f\right) . \tag{7}$$

In our design, the focal length is f=15 mm, and the pixel size is 432 μm × 432 μm, with a total of 30 × 30 phase points. Through full wave simulation of the metasurface, the obvious focusing effect of incident plane waves on the focal plane is observed. Figure 5(d) shows the simulation results in the xoz plane, where the incident wave is x-polarized and the y-polarized component in the transmitted wave is significantly stronger. Similarly, in Fig. 5(e) and 5(f), we present the electric field intensity of the x- and y-polarized waves in the xoy plane (actual focal plane is z=14 mm), respectively. This result presents the focused beam while the polarization plane is rotated 90 degrees. In the experiment, we prepared all-silicon metasurfaces using the method that is same as Fig. 3. Figure 5(g) shows SEM images for the sample, with white boxes marking some of the super-units. Finally, we conduct the measurement of focused beam using a terahertz near-field system, scanning terahertz electric fields for both x- and y-polarized components in the focal plane. The experimental results (at 1.08 THz) are shown in Fig. 5(h) and 5(i), which are basically consistent with the simulation results. Additionally, we calculate the focusing efficiency based on the data in Fig. 5(f) and 5(i), the results indicate that the efficiency values for simulation and experiment are η_s=45.9% and η_e=25.7%, respectively. The focusing efficiency of our racemic metasurface is not as high as many other reports, after all, we use four meta-atoms as a phase pixel. The difference between the two efficiency values may be mainly caused by the low signal-to-noise ratio of the measurement results. The near-field TDS system we use is shown in Fig. 5(j), consisting of terahertz emitter, lens, polarizer and microprobe. The detection of different polarization components in the transmitted beam is achieved by replacing the microprobe. The above results effectively demonstrate the powerful terahertz wave manipulation ability of racemic metasurfaces. In addition, as the enantiomers in the “super-units” provide left- and right-handed circularly polarized components with specific phase differences, the racemic metasurface may serve as a new polarization multiplexing method for devices such as multifunctional meta-lenses and holographic plates, as well as for vector beam generation.

Conclusions

In conclusion, we have demonstrated a new scheme for polarization and wavefront control of terahertz wave based on racemic dielectric metasurfaces, both on simulation and experiment. To alleviate the interference between CD and OA in ordinary chiral metasurfaces, we use the combination of chiral isomers to form a "super-unit" instead of using a single meta-atom as the minimum working unit. Firstly, we obtained an S-shaped structure with strong chiral response through parameter optimization and processed two isomer samples for experimental verification. We built a polarization resolved TDS system to complete transmission spectrum measurement. Then, we mix and arrange the validated chiral meta-atoms to form a new working unit and introduce

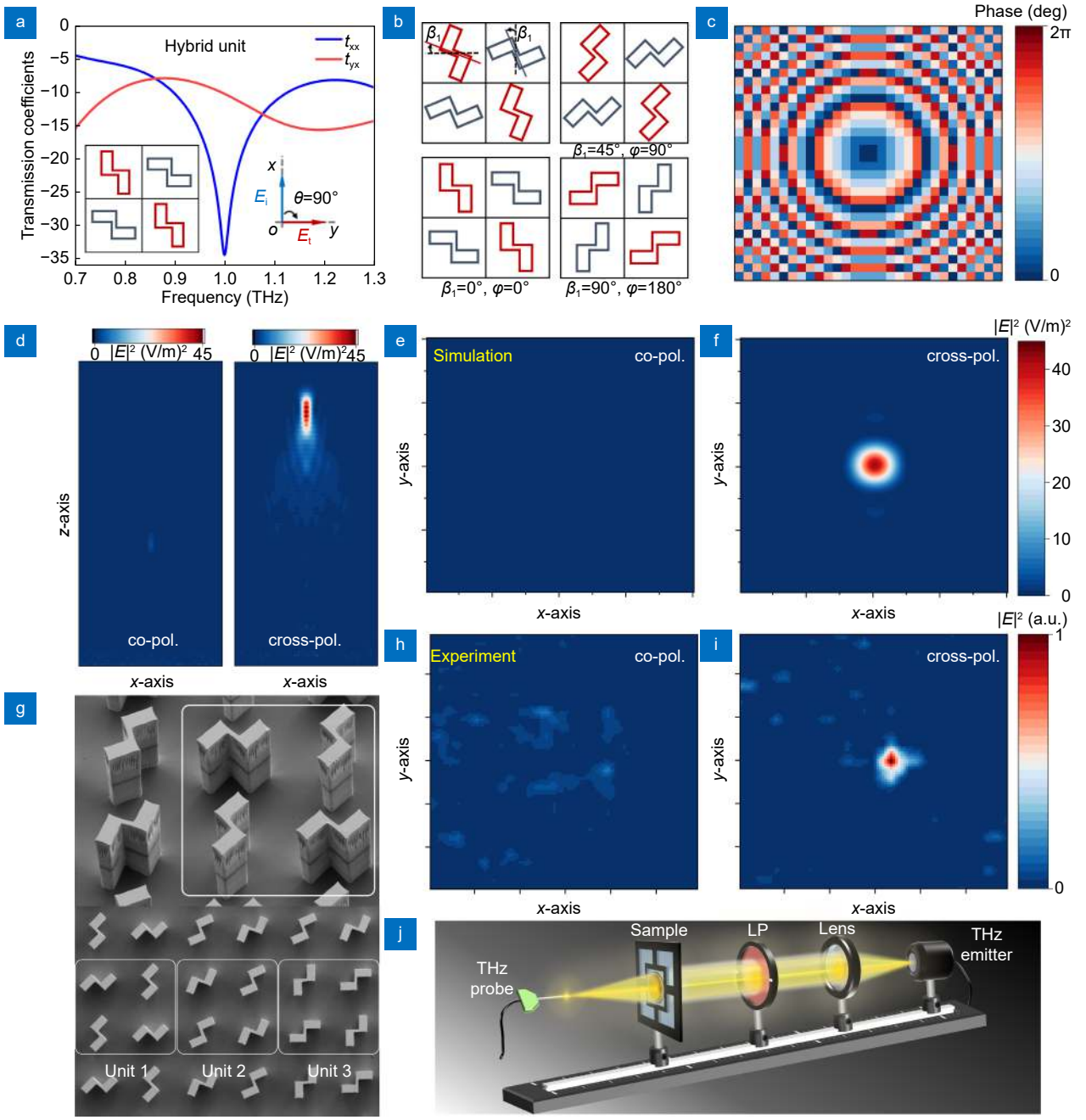

Fig. 5 | (**a**) Simulated linearly polarized transmission spectra of the super-unit arrays (β=90°). (**b**) Example for generating relative phase between super-units (with common rotation angle β_1=0, 45, 90°). (**c**) Design of the metasurface phase profile for beam focusing. (**d**) Simulation results of the focused beam in longitudinal cross-section (*xoz* plane). (**e**, **f**) Simulation results of the focused beam in transverse cross-section (*xoy* plane). (**g**) Localized SEM images of the racemic dielectric metasurface. (**h**, **i**) Experimental results of focused beam in transverse cross-section. (**j**) Experimental optical path for measuring focused terahertz beam.

P-B phase between the atoms (which is called the first-order geometric phase) to obtain a polarization rotation angle. To design the wavefront of the transmitted beam, we next introduced an additional P-B phase between the super-units, i.e. second-order geometric phase. We further validated the wavefront control function of the hybrid metasurface through simulation of the whole sample and measurement of the transmitted focused beam within the focal plane. Our scheme effectively unlocks the CD and OA of chiral metasurfaces while maintaining the wavefront design and also separates the correlation between near-field and far-field chirality of a metadevice, which is of great significance for optical field manipulation and chiral sensing. In terms of light field

manipulation, simultaneous control of chiral near-field and far-field can be used for image encryption and multiplexing display. For optical sensing, Racemic metasurfaces can enhance the chirality of the analyte while eliminating background signals, making sensing more accurate.

References

1. Hao Y, Xiang SY, Han GQ et al. Recent progress of integrated circuits and optoelectronic chips. *Sci China Inf Sci* **64**, 201401 (2021).
2. Tan DZ, Wang Z, Xu BB et al. Photonic circuits written by femtosecond laser in glass: improved fabrication and recent progress in photonic devices. *Adv Photonics* **3**, 024002 (2021).
3. Khorasaninejad M, Capasso F. Metalenses: versatile multifunctional photonic components. *Science* **358**, eaam8100 (2017).
4. Fu R, Chen KX, Li ZL et al. Metasurface-based nanoprinting: principle, design and advances. *Opto-Electronic Sci* **1**, 220011 (2022).
5. Genevet P, Capasso F, Aieta F et al. Recent advances in planar optics: from plasmonic to dielectric metasurfaces. *Optica* **4**, 139–152 (2017).
6. Lin DM, Fan PY, Hasman E et al. Dielectric gradient metasurface optical elements. *Science* **345**, 298–302 (2014).
7. Liu XY, Zhang JC, Leng BR et al. Edge enhanced depth perception with binocular meta-lens. *Opto-Electron Sci* **3**, 230033 (2024).
8. Zhang F, Guo YH, Pu MB et al. Meta-optics empowered vector visual cryptography for high security and rapid decryption. *Nat Commun* **14**, 1946 (2023).
9. Li J, Zheng CL, Li JT et al. Terahertz wavefront shaping with multi-channel polarization conversion based on all-dielectric metasurface. *Photonics Res* **9**, 1939–1947 (2021).
10. Li J, Li JT, Yue Z et al. Structured vector field manipulation of terahertz wave along the propagation direction based on dielectric metasurfaces. *Laser Photonics Rev* **16**, 2200325 (2022).
11. Solntsev AS, Agarwal GS, Kivshar YS. Metasurfaces for quantum photonics. *Nat Photonics* **15**, 327–336 (2021).
12. Wang Q, Tu CH, Li YN et al. Polarization singularities: progress, fundamental physics, and prospects. *APL Photonics* **6**, 040901 (2021).
13. Kang M, Zhang ZY, Wu T et al. Coherent full polarization control based on bound states in the continuum. *Nat Commun* **13**, 4536 (2022).
14. Fan KB, Shadrivov IV, Padilla WJ. Dynamic bound states in the continuum. *Optica* **6**, 169–173 (2019).
15. Huang C, Zhang C, Xiao SM et al. Ultrafast control of vortex microlasers. *Science* **367**, 1018–1021 (2020).
16. Zhang XD, Liu YL, Han JC et al. Chiral emission from resonant metasurfaces. *Science* **377**, 1215–1218 (2022).
17. Chen Y, Feng JG, Huang YQ et al. Compact spin-valley-locked perovskite emission. *Nat Mater* **22**, 1065–1070 (2023).
18. Kim S, An SC, Kin Y et al. Chiral electroluminescence from thin-film perovskite metacavities. *Sci Adv* **9**, eadh0414 (2023).
19. Chen Y, Du W, Zhang Q et al. Multidimensional nanoscopic chiroptics. *Nat Rev Phys* **4**, 113–124 (2022).
20. Chen YX, Zhang FY, Dang ZB et al. Chiral detection of biomolecules based on reinforcement learning. *Opto-Electron Sci* **2**, 220019 (2023).
21. Bu YH, Ren XS, Zhou J et al. Configurable circular-polarization-dependent optoelectronic silent state for ultrahigh light ellipticity discrimination. *Light Sci Appl* **12**, 176 (2023).
22. Guo YH, Zhang SC, Pu MB et al. Spin-decoupled metasurface for simultaneous detection of spin and orbital angular momenta via momentum transformation. *Light Sci Appl* **10**, 63 (2021).
23. Niu CN, Wang ZJ, Zhao J et al. Photonic heterostructures for spin-flipped beam splitting. *Phys Rev Appl* **12**, 044009 (2019).
24. Duan QL, Zeng YL, Yin YH et al. Photonic crystal slabs with maximal chiroptical response empowered by bound states in the continuum. *Photonics Res* **11**, 1919–1933 (2023).
25. Kim RM, Huh JH, Yoo S et al. Enantioselective sensing by collective circular dichroism. *Nature* **612**, 470–476 (2022).
26. Panchenko E, Cadusch JJ, James TD et al. Plasmonic metasurface-enabled differential photodetectors for broadband optical polarization characterization. *ACS Photonics* **3**, 1833–1839 (2016).
27. Li J, Li JT, Zheng CL et al. Lossless dielectric metasurface with giant intrinsic chirality for terahertz wave. *Opt Express* **29**, 28329–28337 (2021).
28. Li JT, Wang GC, Yue Z et al. Dynamic phase assembled terahertz metalens for reversible conversion between linear polarization and arbitrary circular polarization. *Opto-Electron Adv* **5**, 210062 (2022).
29. Li J, Zhang YT, Li JN et al. Amplitude modulation of anomalously reflected terahertz beams using all-optical active Pancharatnam-Berry coding metasurfaces. *Nanoscale* **11**, 5746–5753 (2019).
30. Gryb D, Wendisch FJ, Aigner A et al. Two-dimensional chiral metasurfaces obtained by geometrically simple meta-atom rotations. *Nano Lett* **23**, 8891–8897 (2023).
31. Yuan YY, Zhang K, Ratni B et al. Independent phase modulation for quadruplex polarization channels enabled by chirality-assisted geometric-phase metasurfaces. *Nat Commun* **11**, 4186 (2020).
32. Chen C, Gao SL, Song WG et al. Metasurfaces with planar chiral meta-atoms for spin light manipulation. *Nano Lett* **21**, 1815–1821 (2021).
33. Zhu L, Xu CT, Chen P et al. Pancharatnam–Berry phase reversal via opposite-chirality-coexisted superstructures. *Light Sci Appl* **11**, 135 (2022).
34. Li ZC, Liu WW, Cheng H et al. Spin-selective full-dimensional manipulation of optical waves with chiral mirror. *Adv Mater* **32**, 1907983 (2020).
35. Ding F, Deng YD, Meng C et al. Electrically tunable topological phase transition in non-Hermitian optical MEMS metasurfaces. *Sci Adv* **10**, eadl4661 (2024).
36. Singh R, Plum E, Menzel C et al. Terahertz metamaterial with asymmetric transmission. *Phys Rev B* **80**, 153104 (2009).
37. Singh R, Plum E, Zhang WL et al. Highly tunable optical activity in planar achiral terahertz metamaterials. *Opt Express* **18**, 13425–13430 (2010).
38. Cong LQ, Singh R. Spatiotemporal dielectric metasurfaces for unidirectional propagation and reconfigurable steering of terahertz beams. *Adv Mater* **32**, 2001418 (2020).
39. Tian Z, Singh R, Han JG et al. Terahertz superconducting plasmonic hole array. *Opt Lett* **35**, 3586–3588 (2010).
40. Gu JQ, Han JG, Lu XC et al. A close-ring pair terahertz metamaterial resonating at normal incidence. *Opt Express* **17**, 20307

(2009).
41. Cong LQ, Pitchappa P, Wang N et al. Electrically programmable terahertz diatomic metamolecules for chiral optical control. *Research* **2019**, 7084251 (2019).
42. Wang WH, Srivastava YK, Tan TCW et al. Brillouin zone folding driven bound states in the continuum. *Nat Commun* **14**, 2811 (2023).
43. Cong LQ, Xu NN, Zhang WL et al. Polarization control in terahertz metasurfaces with the lowest order rotational symmetry. *Adv Opt Mater* **3**, 1176–1183 (2015).
44. Cong LQ, Xu NN, Han JG et al. A tunable dispersion-free terahertz metadevice with pancharatnam-berry-phase-enabled modulation and polarization control. *Adv Mater* **27**, 6630–6636 (2015).
45. Menzel C, Rockstuhl C, Lederer F. Advanced Jones calculus for the classification of periodic metamaterials. *Phys Rev A* **82**, 053811 (2010).
46. Nastyshyn SY, Bolesta IM, Tsybulia SA et al. Optical spatial dispersion in terms of Jones calculus. *Phys Rev A* **100**, 013806 (2019).

Acknowledgements

This work was supported by the Scientific Research Foundation of Chengdu University of Information Technology (No. KYTZ202245); Information Materials and Device Applications Key Laboratory of Sichuan Provincial Universities (No. 2023XXCL002); the Key Research and Development Project of Sichuan Province: Research on Development and Application Technology of VO_2 Nano powder/Slurry with Intelligent Temperature Control (Subproject No. 2022Z091); Sichuan Science and Technology Program (No. 2023ZYD0020); National Natural Science Foundation of China (No. 62201378, 12364045, 12304420); Natural Science Foundation of Jiangxi Province (No. 20232BAB211025 and 20232BAB201040); Young Elite Scientists Sponsorship Program by JXAST (No. 2023QT11).

Author contributions

J. Li and H. Xu conceived the idea. J. Li and X. G. Lu fabricated the device and implemented the experiments. J. Li and H. Xu performed the numerical simulations. S. Y. Xiao, H. Li, C. Y. Song, Y. He, J. Y. Liu helped with the data measurement. L. Luo, T. T. Tang, Y. Zhang, Y. T. Zhang helped with the theoretical analysis. S. Y. Xiao and T. T. Liu helped with picture drawing. H. Xu, and H. Li discussed the results and wrote the manuscript. H. Xu, W. X. Huang, Y. Shen and J. Q. Yao supervised the work.

Competing interests

The authors declare no competing financial interests.

Supplementary information

Supplementary information for this paper is available at https://doi.org/10.29026/oea.2024.240075

Scan for Article PDF